Received 31 December 2025; revised 31 January 2026; accepted 8 February 2026. Date of publication 16 February 2026; date of current version 2 March 2026. The review of this article was arranged by Associate Editor Dmitri Vinnikov.

Digital Object Identifier 10.1109/OJPEL.2026.3665487

MPC-Based Power Management for Energy Efficiency and Li-Ion Battery Degradation Mitigation in Off-Grid Hybrid Photovoltaic Inverters

EZEQUIEL GONSCHOROWSKI [1], RAFAEL CARDOSO [1], EDIVAN LAERCIO CARVALHO [2,3], CARLOS MARCELO DE OLIVEIRA STEIN [1], EMERSON GIOVANI CARATI [1], GUSTAVO WEBER DENARDIN [1], AND JEAN PATRIC DA COSTA [1]

[1] Federal University of Technology - Paraná (UTFPR), Pato Branco - PR 85503-390, Brazil
[2] Tallinn University of Technology, 19086 Tallinn, Estonia
[3] NOVA School of Science and Technology, 2829-516 Caparica, Portugal

CORRESPONDING AUTHOR: EZEQUIEL GONSCHOROWSKI (e-mail: gonschorowski@alunos.utfpr.edu.br)

This work was supported in part by the Coordenação de Aperfeiçoamento de Pessoal de Nível Superior - Brasil (CAPES) - Finance Code 001 under Grant ROR identifier: 00x0ma614, in part by the Conselho Nacional de Desenvolvimento Científico e Tecnológico (CNPq) under Grant 405700/2021-0, Grant 306633/2022-1, and Grant 444373/2024-1, in part by NAPI-Sudoeste, Fundação Araucária, in part by UTFPR Campus Pato Branco, in part by Estonian Research Council under Grant PRG3054 and Grant PRG1086, in part by the Estonian Centre of Excellence in Energy Efficiency, ENER, funded by the Estonian Ministry of Education and Research under Grant TK230, in part by research conducted using the research infrastructure “Energy efficiency and renewable energy research infrastructure” funded by Estonian Research Council under Grant TARISTU24-TK12, and in part by the Article Processing Charges (APCs) are covered by the IEEE-CAPES institutional agreement.

ABSTRACT Efficient power management in Hybrid Energy Storage Systems (HESS) for off-grid PV inverters remains a challenge, particularly in terms of energy efficiency and battery degradation mitigation. In this context, this paper proposes a Model Predictive Control (MPC) based power management designed to mitigate Li-ion battery degradation while improving the overall system efficiency. To validate this proposal, extensive experimental results are presented. The proposed formulation aims to minimize battery stress by smoothing the current profile and reducing cycling effects. The performance of the MPC power management is verified through a comparative experimental analysis of four distinct strategies: rule-based, frequency-filtering, a benchmark MPC, and the proposed MPC. Evaluation is based on four key metrics: RMS current, total power losses, Equivalent Full Cycles (EFC), and State of Health variation (ΔSOH). Experimental results demonstrate that the proposed method outperforms the compared strategies across all evaluated criteria, significantly reducing battery stress in terms of cycling and current distribution. Furthermore, long-term simulations corroborate these findings, showing a substantial reduction in battery degradation compared to other established methods. These results confirm that the proposed method, provides a robust solution for mitigating battery degradation in hybrid inverter applications.

INDEX TERMS Off-grid photovoltaic hybrid inverter, hybrid energy storage system, li-ion battery, supercapacitor.

I. INTRODUCTION

Growing concerns about environmental sustainability have accelerated the adoption of renewable energy sources. In this context, dc microgrids, as well as hybrid inverters integrating photovoltaics and energy storage, have emerged as innovative solutions, due to their ability to enhance the reliability of energy systems [1], [2]. In particular, isolated dc microgrids have emerged as a key option for increased reliability, resilience, and autonomy in energy systems [3], [4].

In the context of off-grid systems with energy storage, including microgrids and residential installations [5], Li-ion batteries are often preferred due to their numerous advantages.

Their high energy density and superior discharge capability make them well-suited for systems requiring reliable and efficient energy storage [6], [7]. Additionally, they offer high efficiency, a long lifespan, and low internal resistance [8]. Furthermore, ongoing advances in battery technology and manufacturing processes have resulted in continuous cost reductions. In the last few years, the price of Li-ion batteries was reported as $139 kWh with a gravimetric energy density of 270 Wh/kg. Projections for 2030 estimate a price reduction to $54 kWh and an increase in gravimetric density to 600 Wh/kg showing a significant advance in batteries technology [9].

Therefore, the integration of Li-ion batteries with photovoltaic (PV) systems has increased in recent years, as their complementary characteristics enable more efficient and reliable energy system, particularly in islanded or off-grid applications [10]. In addition, Li-ion batteries can also be combined with supercapacitors to further enhance energy utilization: the battery provides high energy density, while the supercapacitor offers high power density. For example, a hybrid photovoltaic inverter can utilize both batteries and supercapacitors to maintain a constant output power. During short-term power fluctuations, the supercapacitors can absorb or supply energy, while for sustained variations, the Li-ion battery provides the necessary energy support. Therefore, the HESS configuration (batteries and supercapacitors) can reduce battery usage by providing a proper Power Management System (PMS) [11].

A PMS is required to ensure the proper coordination of the storage elements and the efficient operation of dc microgrids, or even simpler systems such as hybrid photovoltaic inverters. The four most common power management methods for HESS are rule-based, frequency-based, data-driven, and optimization-based [12].

The rule-based approach establishes power management rules based on experience and user needs. The frequency-based approach decomposes the HESS power demand into low and high-frequency components, distributing them based on the characteristics of the storage elements. The optimization method aims to determine the optimal power management solution based on specific objective criteria. The data-driven approach uses concepts of artificial intelligence (AI) to solve the power management problem [12].

In [13], a rule-based approach was implemented for a hybrid inverter employing a battery and a supercapacitor. The primary objective is to prioritize the supercapacitor for charging and discharging whenever possible. However, a significant limitation is that the power management strategy renders the supercapacitor unavailable too quickly. Consequently, the battery is forced to handle all power demand variations, including high-frequency fluctuations, which is undesirable. In [14], a different approach was demonstrated, using a virtual price concept that varies with the DC bus voltage level. A voltage above a specific threshold indicates excess energy, while undervoltage represents an energy deficit. The storage elements charge or discharge in response to these price variations. However, a key limitation of this approach is its lack of support for battery state-of-charge (SOC) management, as the strategy does not discourage unnecessary Li-ion battery cycling and may even lead to increased cycling.

A frequency-based approach is presented in [15]. A low-pass filter is used to dynamically distribute energy between the lithium-ion battery and supercapacitor in an off-grid hybrid inverter. To calculate the filter's cutoff frequency, the SOC and State of Power (SOP) of the battery are used. The approach reduces the battery's Root Mean Square (RMS) current, thereby decreasing stress on the battery and increasing its lifespan. Similarly, in [16], a frequency-based management is proposed for an off-grid hybrid inverter, which differs in the power management. The proposal employs a Fractional-Order Proportional-Integral (FOPI) controller to regulate the DC bus voltage. The controller's output determines the total reference current for the storage system, which is then decomposed by a fixed low-pass filter to allocate power between the battery and the supercapacitor. A significant issue with the frequency-based strategy is power loss in the HESS and Li-ion battery cycling, as this approach does not directly address these factors.

In [17], a data-driven approach is presented utilizing a Long Short-Term Memory (LSTM) network trained via Proximal Policy Optimization (PPO). The system can learn charging and discharging policies from historical data. This management strategy governs the allocation of energy between the grid, the storage system, and local loads. However, the limitations of this approach include the assumption that the system is a fixed model, the need for a large volume of training data, and constraints on the optimization window. Furthermore, battery lifespan can be compromised when the strategy prioritizes profit maximization. In [18], a Robust Variational Physics-Informed Neural Network (RVPNN) is presented. This machine learning strategy leverages physics concepts related to the system, which comprises a fuel cell, a battery, and a supercapacitor. The RVPNN regulates the system's DC bus voltage by predicting control signals. However, this approach is highly complex, and the degradation of the Li-ion battery is not accounted for in the formulation.

In the optimization approach, Model Predictive Control (MPC) has been used for Hybrid Energy Storage Systems (HESS). It is used in Electric Vehicles (EVs) [19], in isolated microgrids with Li-ion batteries and fuel cells [20], and a hybrid inverter grid-connected [21] to reduce electricity costs. However, few studies using MPC for off-grid microgrid systems using Li-ion batteries and supercapacitors are available. In [22], [23], the authors present a formulation of the MPC where only the SOC of the supercapacitor is considered in the cost function. In [24], a dual-layer MPC strategy is proposed for a PV-based microgrid, where a primary MPC calculates the power balance and a secondary MPC provides current references for the HESS. In [25], an MPC is presented for calculating the necessary current for regulating the power balance of the HESS, and this current is decomposed using fuzzy logic to set the references for the battery and supercapacitor. These previous works do not experimentally validate the management strategies or do not use real case scenarios.

To address the drawbacks of previous strategies, this paper proposes a new power management system based on Model Predictive Control (MPC). This concept was initially introduced as preliminary work in [11]. However, the complexity of the subject and the availability of additional experimental results motivate an extended version for this journal publication. Therefore, the main contribution of this work is to expand the controller formulation presented in the conference paper, specifically by incorporating the HESS power loss terms into the MPC cost function. These additional variables aim to mitigate operational degradation of Li-ion batteries by minimizing usage cycles and reducing power dissipation, thereby enhancing the system's overall energy management. Furthermore, all results presented in this paper are obtained from an experimental test bench that has not been previously reported.

This work contributes both an MPC formulation and a comprehensive experimental framework for power management in HESS. The proposed strategy is evaluated against three established approaches: a rule-based strategy [26], a frequency-based strategy [15], and a benchmark MPC [23]. This latter method was selected because it represents a recent contribution that focuses on the supercapacitor's state of charge within the MPC formulation, providing a clear contrast to the strategy proposed in this work. Unlike studies limited to theoretical analysis, this research provides a comparative study based on four distinct experimental implementations, analyzing performance through RMS current, power losses, Equivalent Full Cycles (EFC), and State of Health variation (ΔSOH). The proposed cost function is designed to mitigate operational battery degradation. Experimental results highlight a significant reduction in battery stress and cycling compared to the benchmark strategies. These findings are further supported by seven-day simulations, which confirm a substantial mitigation of battery degradation. This combination of an optimized cost function and rigorous experimental validation confirms the effectiveness of the proposed system in minimizing the physical stress factors that lead to Li-ion battery degradation.

The remainder of this paper is organized as follows: Section II details the system description. Section III discusses the battery modeling and the battery's State of Charge (SOC) determination using an Extended Kalman Filter (EKF), which are both required by the MPC. Section IV presents the mathematical formulation of the MPC power management and explains how the controller interacts with the overall system. Section V provides the experimental results and a comparative analysis of the MPC against other strategies. Finally, Section VI presents the conclusions and discusses the implications of this work.

II. SYSTEM DESCRIPTION

Fig. 1 illustrates the structure of the hybrid photovoltaic inverter, which is composed of four converters. The first is the Photovoltaic (PV) system converter. This converter extracts power from the PV system using a Maximum Power Point Tracking (MPPT) or Limited Power Point Tracking (LPPT) algorithm [27].

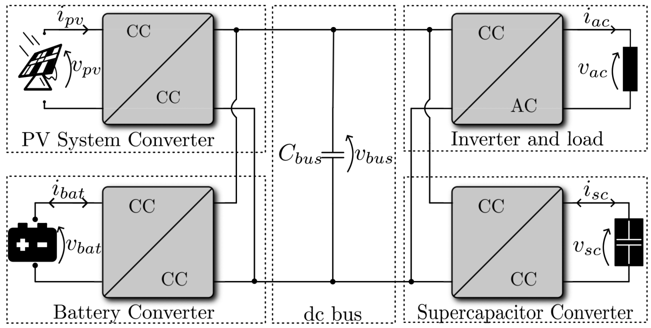

FIGURE 1. Schematic diagram of the hybrid photovoltaic inverter system.

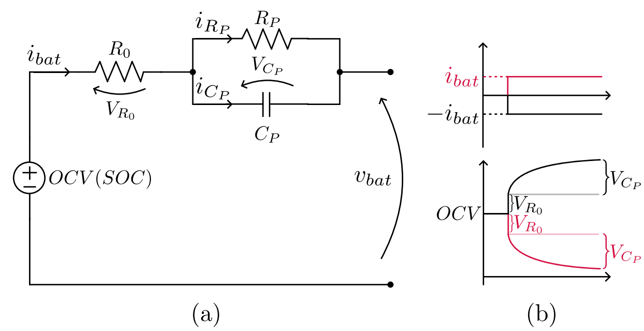

FIGURE 2. 1RC equivalent circuit model for the Li-ion battery.

The second converter is a bidirectional converter interfacing the supercapacitor bank and the dc bus capacitor. This converter manages the charging and discharging cycles of the supercapacitor. The third converter is another bidirectional converter associated with the battery. It regulates the DC bus voltage by charging or discharging the battery. Finally, the inverter supplies AC power to the load by converting the DC power from the bus. The complete system structure is explained in more detail in [28], where all control loops and the design are demonstrated.

III. BATTERY MODELING AND *SOC* DETERMINATION

To implement the proposed MPC strategy, a battery's equivalent circuit model (ECM) representation of the battery dynamics is required, along with the State of Charge (SOC), which represents the battery's available energy. Since the SOC is a non-measurable variable, it is provided by an Extended Kalman Filter (EKF) that also uses the battery's ECM. The EKF is adopted as a reliable tool to handle the nonlinearities of the battery model, particularly the relationship between SOC and Open Circuit Voltage (OCV). The methodology used to provide de SOC at each sampling time is described in [29].

The ECM of the battery is represented in Fig. 2. The following equation characterizes the battery dynamics:

$$V_{C_{P_{k+1}}} = \left(1 - \frac{T_s}{C_P R_P}\right) V_{C_{P_k}} + \frac{T_s}{C_P} i_{bat_k}, \tag{1}$$

where T_s is the sampling time, and the electrical parameters are defined according to the model in Fig. 2.

The battery terminal voltage is given by

$$v_{bat_k} = OCV(SOC_k) - V_{CP_k} - R_0 i_{bat_k}, \tag{2}$$

where $OCV(SOC_k)$ is a polynomial representing the OCV as a function of the State of Charge [30]. While third or seventh order polynomials are frequently utilized in the literature, a fifth-order model is adopted in this work to balance accuracy and computational complexity. Consequently, the battery terminal voltage v_{bat_k} is expressed as:

$$v_{bat_k} = \sum_{i=0}^{5} a_i SOC_k^i - V_{CP_k} - R_0 i_{bat_k}. \tag{3}$$

The $OCV(SOC_k)$ function is linearized using a Taylor series expansion around the operating point $\overline{SOC}_k$, yielding:

$$\begin{aligned} OCV(SOC_k) &\approx \sigma_{1_k} SOC_k + \sigma_{2_k}, \\ \sigma_{1_k} &= \sum_{i=1}^{n} a_i i \overline{SOC}_k^{i-1}, \\ \sigma_{2_k} &= \sum_{i=0}^{n} a_i \overline{SOC}_k^{i} - \sigma_{1_k} \overline{SOC}_k. \end{aligned}$$

Finally, v_{bat_k} can be written in its linearized form:

$$v_{bat_k} = \left(\sigma_{1_k} SOC_k + \sigma_{2_k}\right) - V_{CP_k} - R_0 i_{bat_k}. \tag{4}$$

The coefficients σ_{1_k} and σ_{2_k} are updated at each time step based on the current SOC observation.

The battery SOC is described as:

$$SOC_{k+1} = SOC_k - \frac{T_s i_{bat_k}}{3600 \cdot Q_{max}}. \tag{5}$$

Positive values of i_{bat_k} indicate the battery discharges, while negative values represent the battery charging.

IV. MPC POWER MANAGEMENT

This section discusses the proposed power management strategy of the hybrid photovoltaic inverter during off-grid operation. The primary objective of this management system is to ensure power delivery to the load, regardless of whether the generated power is insufficient or exceeds demand, while extending the life span by mitigating lithium-ion battery degradation and conserving energy within the storage elements.

The proposed PMS employs Model Predictive Control (MPC). This optimal control technique predicts the system's output using a cost function and a system model to determine the most effective control action, while accounting for constraints on predicted outputs and control actions [31]. Therefore, to implement the proposed MPC power management system, an adequate cost function and a dynamic model of the system must be developed. Additionally, physical restrictions on the outputs and control actions must be considered. Finally, the optimization problem is solved, yielding the optimal control action. These topics are discussed in the following sections.

A. COST FUNCTION

The cost function determines how the MPC calculates control actions to meet the desired objectives, enabling the system to operate considering predefined constraints. The cost function used in this work is expressed as:

$$\begin{aligned} J_{mpc_k} = \alpha_1 & \underbrace{\left[(P_{l_k} - P_{pv_k}) - (P_{bat_k} + P_{sc_k})\right]^2}_{1^{st}\ term} \\ & + \alpha_2 \underbrace{(\beta_{SOC} - SOC_k)^2}_{2^{nd}\ term} + \alpha_3 \underbrace{(\beta_{SOC_{sc}} - SOC_{sc_k})^2}_{3^{rd}\ term} \\ & + \alpha_4 \underbrace{(\beta_{P_{R_0}} - R_0 i_{bat_k}^2)^2}_{4^{th}\ term} + \alpha_5 \underbrace{(\beta_{P_{R_{sc}}} - R_{sc} i_{sc_k}^2)^2}_{5^{th}\ term} \\ & + \underbrace{\Delta i_{hess_k}^T K \Delta i_{hess_k}}_{6^{th}\ term}. \end{aligned} \tag{6}$$

In the first term of the cost function presented in (6), the difference between the load power (P_{l_k}) and the power from the photovoltaic panels (P_{pv_k}) acts as the reference power for the total power the HESS must provide to balance the power in the system, that is, $P_{bat_k} + P_{sc_k}$, where P_{bat_k} and P_{sc_k} are the power provided by the battery and supercapacitor, respectively. When $(P_{l_k} - P_{pv_k})$ is positive, the photovoltaic power generation (P_{pv_k}) is lower than the load demand. The HESS must discharge to supply the power difference through the battery (P_{bat}) and the supercapacitor (P_{sc_k}). Conversely, when the term is negative, the generated power exceeds the load demand, and the HESS is charged accordingly.

The second and third terms of the cost function are associated with the desired State of Charge (SOC) of the battery (SOC_{bat}) and the supercapacitor (SOC_{sc}). These terms promote charging the battery and discharging the supercapacitor when the reference values are set to $\beta_{SOC_k} = 1$ and $\beta_{SOC_{sc_k}} = 0.01$. Since the battery has a high energy density while the supercapacitor has a low energy density, it is suitable to use the battery as an energy backup during periods of low irradiance or at night. In contrast, due to its high power density, the supercapacitor is better suited for compensating for power fluctuations during the day.

The fourth term addresses two key concepts: first, it minimizes the irreversible power dissipation in the Li-ion battery to enhance system efficiency and, second, it aims to extend the battery's lifespan. By minimizing this term, the MPC reduces current stress and cycle usage. Specifically, this term represents the Joule heating ($R_0 i_{bat}^2$), which is the primary controllable driver of the battery's thermal behavior. Although heat generation also includes a reversible (entropic) component, it is not explicitly modeled here due to its secondary impact on control decisions at the low C-rates investigated and the high uncertainty in its parametrization.

Within this MPC framework, the internal temperature is treated as a physical consequence of the dissipated power rather than a directly controlled state; therefore, by minimizing this term, the controller indirectly mitigates thermal stress, undesirable internal reactions, and structural electrode degradation, while maintaining high Coulombic efficiency through low internal polarization [32]. Similarly, the fifth term accounts for the power dissipated in the supercapacitor, ensuring that the combined minimization of these terms reduces the total power dissipation within the HESS and improves the system's overall energy efficiency.

The sixth term corresponds to the variation of control actions. It represents the variation in battery and supercapacitor currents (HESS currents). By controlling these variations, the MPC can manage the system's power while adhering to the formulation in the cost function (6). The HESS current variation vector calculated by the MPC is defined as:

$$\Delta i_{hess_k} = \begin{bmatrix} \Delta i_{bat_k} & \Delta i_{sc_k} \end{bmatrix}^T, \tag{7}$$

where Δi_{bat_k} and Δi_{sc_k} are the battery and the supercapacitor current variations, respectively. The MPC computes these variations to determine the updated control actions:

$$i_{bat_{k+1}} = \Delta i_{bat_k} + i_{bat_k}, \tag{8}$$

$$i_{sc_{k+1}} = \Delta i_{sc_k} + i_{sc_k}. \tag{9}$$

The weights $\alpha_1, \ldots, \alpha_5$ and the matrix K are adjusted to penalize specific terms in the cost function. When a weight is increased, the MPC gives the associated term greater importance in the optimization, thereby restricting its use. The opposite occurs when a weight is reduced. As previously discussed, the strategy prioritizes the use of the supercapacitor over the Li-ion battery to extend the latter's lifespan. Consequently, the weight associated with the battery (α_4) is assigned the highest significance, as it directly penalizes the battery's power dissipation and dictates its current profile. This weight is chosen after heuristic tests and improves the metrics compared in Section V.

Each term in the cost function possesses a distinct physical significance and influences the MPC optimization process differently. The first term represents the HESS power balance and inherently exerts a higher impact on the total cost due to its larger numerical magnitude, especially when compared to the second and third terms (battery and supercapacitor) state of charge, which are normalized between 0 and 1. The fifth and sixth terms represent power dissipation and control effort, respectively, and are assigned secondary importance within the optimization priority.

To ensure the controller effectively addresses battery longevity, the weighting factor α_4 is set to 200. This choice serves to normalize and augment the relative contribution of the battery power loss term, ensuring that degradation mitigation is prioritized alongside power tracking. Consequently, while the MPC seeks to satisfy all objectives, the tracking of secondary references (such as the 2nd, 3rd, and 5th terms) may not be perfect, reflecting the inherent trade-offs of the multi-objective HESS power management.

The proposed MPC does not account for the State of Health (SOH) of the supercapacitor because its high power density allows a high variation in the current profile. Compared to the battery, the supercapacitor has numerous cycles, on the order of 10^6.

B. SYSTEM MODELING

To implement the MPC, the 1^{st}, 2^{nd}, 3^{rd}, 4^{th}, and 5^{th} terms in (6) must be expressed using a state-space representation of the form

$$x_{k+1} = Ax_k + Bu_k, \tag{10}$$

$$y_k = Cx_k + \varphi_k, \tag{11}$$

where φ_k represents the constant terms required to formulate the output equation.

For this purpose, the state vector is defined as:

$$x_{mpc_k} = \begin{bmatrix} V_{CP_k} & SOC_k & i_{bat_k} & i_{sc_k} & v_{sc_k} \end{bmatrix}^T. \tag{12}$$

The variable V_{CP_k} represents the voltage across the polarization capacitor in the battery model defined in (1). The SOC denotes the battery State of Charge, as defined in (5). The battery current (i_{bat}) and supercapacitor current (i_{sc}) are defined by (8) and (9), respectively. Consequently, the state equations for these currents are expressed as:

$$\begin{aligned} i_{bat_{k+1}} &= i_{bat_k} + \Delta i_{bat_k}, \\ i_{sc_{k+1}} &= i_{sc_k} + \Delta i_{sc_k}. \end{aligned} \tag{13}$$

The voltage of the supercapacitor evolves according to the following equation:

$$v_{sc_{k+1}} = v_{sc_k} - \frac{T_s}{C_{sc}} i_{sc_k}. \tag{14}$$

Therefore, the state equation of the system is given by:

$$\underbrace{\begin{bmatrix} V_{CP_{k+1}} \\ SOC_{k+1} \\ i_{bat_{k+1}} \\ i_{sc_{k+1}} \\ v_{sc_{k+1}} \end{bmatrix}}_{x_{mpc_{k+1}}} = \underbrace{\begin{bmatrix} 1-\frac{T_s}{\tau_{P_k}} & 0 & \frac{T_s}{C_{P_k}} & 0 & 0 \\ 0 & 1 & \frac{-T_s}{3600Q_{\max}} & 0 & 0 \\ 0 & 1 & 0 & 0 & 0 \\ 0 & 0 & 1 & 0 & 0 \\ 0 & 0 & 0 & \frac{-T_s}{C_{sc}} & 1 \end{bmatrix}}_{A_{mpc}} \underbrace{\begin{bmatrix} V_{CP_k} \\ SOC_k \\ i_{bat_k} \\ i_{sc_k} \\ v_{sc_k} \end{bmatrix}}_{x_{mpc_k}}$$

$$+ \underbrace{\begin{bmatrix} 0 & 0 \\ 0 & 0 \\ 1 & 0 \\ 0 & 1 \\ 0 & 0 \end{bmatrix}}_{B_{mpc}} \Delta i_{HESS_k} \tag{15}$$

To define the output state-space equation, initially, its first output, that appears in the first term of (6), is defined as:

$$P_{bat_k} + P_{sc_k} = v_{bat_k} i_{bat_k} + v_{sc_k} i_{sc_k}, \tag{16}$$

where i_{bat_k}, i_{sc_k}, and v_{sc_k} are directly measured state variables, while v_{bat_k}, as defined in (4), is a function of the states SOC_k, i_{bat_k}, and V_{CP_k}, and needs to be linearized with respect to the state variables to be written in the form of (11).

The second defined output, present in the second term of (6), represents the state of charge of the battery (SOC) and is defined by (5). It is linear with respect to the state variables.

The state of charge of the supercapacitor (SOC_{sc}), appearing in the third term, is given by:

$$SOC_{sc_k} = \frac{E_{act_k}}{E_{max}}, \tag{17}$$

where E_{act_k} represents the instantaneous energy stored in the supercapacitor and E_{max} is its maximum energy capacity. Considering that the energy stored in a capacitor is defined as $E = \frac{1}{2}Cv^2$, the SOC of the supercapacitor can be expressed as:

$$SOC_{sc_k} = \frac{v_{sc_k}^2}{v_{sc_{max}}^2}. \tag{18}$$

The fourth and fifth terms represent the power dissipation in the battery and supercapacitor of the HESS. They are given by $P_{R0_k} = R_0 i_{bat_k}^2$ and $P_{Rsc_k} = R_{sc} i_{sc_k}^2$, respectivelly. Since both terms are non-linear with respect to the states i_{bat_k} and i_{sc_k}, they must be linearized as functions of these states.

The linearization of the aforementioned equations is based on the Taylor expansion, and it is given by:

$$f(x) \approx f(\bar{a}) + f'(\bar{a})(x - \bar{a}), \tag{19}$$

where $\bar{a}$ is the operating point used for linearization.

At each sampling time k, P_{bat_k}, P_{sc_k}, SOC_{sc_k}, P_{R0_k} and P_{Rsc_k} are linearized around the current operating point $[\bar{V}_{CP}, \overline{SOC}, \bar{i}_{bat}, \bar{i}_{sc}, \bar{v}_{sc}]_k$. Consequently, the linearized expressions are defined as:

$$\underbrace{\begin{bmatrix} P_{bat_k} + P_{sc_k} \\ SOC_k \\ SOC_{sc_k} \\ P_{R0_k} \\ P_{Rsc_k} \end{bmatrix}}_{y_{mpc_k}} = \underbrace{\begin{bmatrix} -\bar{i}_{bat} & \sigma_{1_k}\bar{i}_{bat} & \Omega_k & \bar{v}_{sc} & \bar{i}_{sc} \\ 0 & 1 & 0 & 0 & 0 \\ 0 & 0 & 0 & 0 & \frac{2\bar{v}_{sc}}{v_{sc\,\max}^2} \\ 0 & 0 & 2R_0\bar{i}_{bat} & 0 & 0 \\ 0 & 0 & 0 & 2R_{sc}\bar{i}_{sc} & 0 \end{bmatrix}}_{C_{mpc_k}} \underbrace{\begin{bmatrix} V_{CP_k} \\ SOC_k \\ i_{bat_k} \\ i_{sc_k} \\ v_{sc_k} \end{bmatrix}}_{x_{mpc_k}} + \underbrace{\begin{bmatrix} \bar{V}_{CP}\bar{i}_{bat} + R_0\bar{i}_{bat}^2 - \sigma_{1_k}\overline{SOC}\bar{i}_{bat} \\ 0 \\ \frac{-\bar{v}_{sc}^2}{v_{sc\,\max}^2} \\ -R_0\bar{i}_{bat}^2 \\ -R_{sc}\bar{i}_{sc}^2 \end{bmatrix}}_{\varphi_k} \tag{20}$$

where $\Omega_k = -\bar{V}_{CP} + \sigma_{2_k} + \sigma_{1_k}\overline{SOC} - 2R_0\bar{i}_{bat}$.

Using (15) and (20), the final state-space representation for the MPC has the following format:

$$\begin{aligned} x_{mpc_{k+1}} &= A_{mpc_k} x_{mpc_k} + B_{mpc_k} \Delta i_{hess_k}, \\ y_{mpc_k} &= C_{mpc_k} x_{mpc_k} + \varphi_k, \end{aligned} \tag{21}$$

where φ_k represents the constant terms resulting from the linearizations.

C. OUTPUT PREDICTION

In the MPC strategy, outputs are predicted using the current state vector x_{mpc_k} and the system matrices A_{mpc_k}, B_{mpc_k}, and C_{mpc_k}. The predicted output vector is given by:

$$Y_{mpc_k} = F_{mpc_k} x_{mpc_k} + \Phi_{mpc_k} \Delta i_{hess_k} + \varphi_{mpc_k}, \tag{22}$$

where F_{mpc_k} and Φ_{mpc_k} are the output prediction matrix and the dynamic prediction matrix, respectively, derived from the state-space matrices A_{mpc_k}, B_{mpc_k}, and C_{mpc_k} of the MPC model:

$$F_{mpc_k} = \begin{bmatrix} C_{mpc_k} A_{mpc_k} \\ C_{mpc_k} A_{mpc_k}^2 \\ \vdots \\ C_{mpc_k} A_{mpc_k}^{N_p} \end{bmatrix},$$

$$\Phi_{mpc_k} = \begin{bmatrix} C_{mpc_k} B_{mpc_k} & 0 & \cdots & 0 \\ C_{mpc_k} A_{mpc_k} B_{mpc_k} & C_{mpc_k} B_{mpc_k} & \cdots & 0 \\ \vdots & \vdots & \ddots & \vdots \\ C_{mpc_k} A_{mpc_k}^{N_p-1} B_{mpc_k} & \cdots & \cdots & C_{mpc_k} A_{mpc_k}^{N_p-N_c} B_{mpc_k} \end{bmatrix}, \tag{23}$$

where N_p is the prediction horizon and N_c is the control horizon.

The term φ_{mpc_k} represents the constant components that arise from the linearization process described in (20), defined as:

$$\varphi_{mpc_k} = \mathbf{1}_{N_p} \otimes \varphi_k, \tag{24}$$

where $\mathbf{1}_{N_p}$ is a column vector of ones with dimension N_p, $\otimes$ denotes the Kronecker product.

D. CONSTRAINS DEFINITION

In the MPC framework, the constraints for the optimization problem are applied to the control action increments, the control action magnitudes, and the predicted outputs. These constraints are expressed in a compact linear inequality form as:

$$M\Delta i_{hess} \leq \gamma, \tag{25}$$

where M is the coefficient matrix that defines the linear relationships of the constraints, and γ is the vector representing the respective upper and lower bounds for all constrained variables throughout the prediction horizon.

The control action variations in the formulated MPC correspond to changes in the HESS currents: the battery current (Δi_{bat}) and the supercapacitor current (Δi_{sc}). The constraints on current variation are defined as:

$$\begin{bmatrix} -\Delta i_{bat_{max}} \\ -\Delta i_{sc_{max}} \end{bmatrix} \leq \begin{bmatrix} \Delta i_{hess} \end{bmatrix} \leq \begin{bmatrix} \Delta i_{bat_{max}} \\ \Delta i_{sc_{max}} \end{bmatrix}, \tag{26}$$

where $\Delta i_{bat_{max}}$ and $\Delta i_{sc_{max}}$ represent the maximum allowable current variations for the Li-ion battery and the supercapacitor, respectively.

The current magnitude constraints for the HESS are defined as:

$$\begin{bmatrix} -i_{bat_{max}} \\ -i_{sc_{max}} \end{bmatrix} \leq \begin{bmatrix} i_{hess} \end{bmatrix} \leq \begin{bmatrix} i_{bat_{max}} \\ i_{sc_{max}} \end{bmatrix}, \tag{27}$$

where $i_{bat_{max}}$ and $i_{sc_{max}}$ represent the maximum current magnitudes for the Li-ion battery and the supercapacitor, respectively.

The system outputs comprise the HESS power demand ($P_{bat_k} + P_{sc_k}$), the state of charge of the battery (SOC) and supercapacitor (SOC_{sc}) and the power dissipated within the HESS, as demonstrated in output (20) of the state-space model. Consequently, the constraints on the predicted outputs are given by:

$$\underbrace{\begin{bmatrix} P_{l_k} - P_{pv_k} \\ SOC_{min} \\ SOC_{sc_{min}} \\ 0 \\ 0 \end{bmatrix}}_{y_{mpc_{min_k}}} \leq \underbrace{\begin{bmatrix} P_{bat_k} + P_{sc_k} \\ SOC_k \\ SOC_{sc_k} \\ P_{R0_k} \\ P_{Rsc_k} \end{bmatrix}}_{y_{mpc_k}} \leq \underbrace{\begin{bmatrix} P_{l_k} - P_{pv_k} \\ SOC_{max} \\ SOC_{sc_{max}} \\ i^2_{bat_{\max}} R_0 \\ i^2_{sc_{\max}} R_{sc} \end{bmatrix}}_{y_{mpc_{max_k}}}. \tag{28}$$

Finally, the predicted output constraints can be formulated as:

$$Y_{mpc_{min_k}} \leq Y_{mpc_k} \leq Y_{mpc_{max_k}}, \tag{29}$$

where

$$Y_{mpc_{min_k}} = \mathbf{1}_{N_p} \otimes y_{mpc_{min_k}},$$
$$Y_{mpc_{max_k}} = \mathbf{1}_{N_p} \otimes y_{mpc_{max_k}}.$$

Combining the equations that describe the restrictions in the magnitude of the variation of the HESS currents, the magnitude of HESS currents, and the magnitude of the predicted outputs, given by (26), (27), and (28), respectively, in restrictions forms for the MPC (25), the final restriction is given by

$$\underbrace{\begin{bmatrix} 1 & \cdots & 0 \\ \vdots & \ddots & \vdots \\ 0 & \cdots & 1 \\ -1 & \cdots & 0 \\ \vdots & \ddots & \vdots \\ 0 & \cdots & -1 \\ 1 & \cdots & 0 \\ \vdots & \ddots & \vdots \\ 1 & \cdots & 1 \\ -1 & \cdots & 0 \\ \vdots & \ddots & \vdots \\ -1 & \cdots & -1 \\ & \Phi_{mpc_k} & \\ & -\Phi_{mpc_k} & \end{bmatrix}}_{M_{mpc}} \begin{bmatrix} \Delta i_{hess_k} \\ \vdots \\ \Delta i_{hess_{N_c-1}} \end{bmatrix}$$

$$\leq \underbrace{\begin{bmatrix} \Delta i_{hess_{max}} \\ \vdots \\ \Delta i_{hess_{max}} \\ \Delta i_{hess_{max}} \\ \vdots \\ \Delta i_{hess_{max}} \\ i_{hess_{max}} - i_{hess_{k-1}} \\ \vdots \\ i_{hess_{max}} - i_{hess_{k-1}} \\ i_{hess_{max}} + i_{hess_{k-1}} \\ \vdots \\ i_{hess_{max}} + i_{hess_{k-1}} \\ Y_{mpc_{\max_k}} - F_{mpc_k} x_{mpc_k} - \varphi_{mpc} \\ -Y_{mpc_{\min_k}} + F_{mpc_k} x_{mpc_k} + \varphi_{mpc} \end{bmatrix}}_{\gamma_{mpc}}, \tag{30}$$

where $\Delta i_{hess_{max}}$ represents the maximum allowable variation in the HESS current, and $i_{hess_{max}}$ denotes the maximum current amplitude. The signs associated with these variables are arranged within matrices M_{mpc} and γ_{mpc}.

E. SOLVING THE MPC

The MPC is solved using Quadratic Programming (QP), transforming the cost function in (6) into a linear tracking problem [33], given by:

$$J_{mpc_k} = \left(R_{s_{mpc_k}} - Y_{mpc_k}\right)^T \chi \left(R_{s_{mpc_k}} - Y_{mpc_k}\right) + \Delta i^T_{hess_k} K \Delta i_{hess_k} \tag{31}$$

where Y_{mpc_k} denotes the predicted output vector, $R_{s_{mpc_k}}$ is the reference trajectory, and K is the weighting matrix for control action variations. Although the matrix χ typically defines tracking weights, as demonstrated in (20), the outputs already include the weighting factors from the initial cost function. To ensure consistency, the output references must also incorporate these weights. Consequently, the system reference vector is defined as:

$$R_{s_k} = \begin{bmatrix} \alpha_1 \left(P_{l_k} - P_{pv_k}\right) & \alpha_2 \beta_{SOC} & \alpha_3 \beta_{SOC_{sc}} & \alpha_4 \beta_{P_{R_0}} & \alpha_5 \beta_{P_{R_{SC}}} \end{bmatrix}^T \tag{32}$$

and the reference trajectory for the predicted outputs is given by:

$$R_{s_{mpc_k}} = \mathbf{1}_{N_p} \otimes R_{s_k}. \tag{33}$$

By doing this, the matrix χ in (31) becomes an identity matrix and can be omitted from the formulation.

The cost function in (31) must be rewritten in the QP format to solve the MPC problem using the QP algorithm. To achieve this, the following process is applied:

$$J_{QP_{mpc_k}} = \Delta i_{hess_k}^T H_{mpc_k} \Delta i_{hess_k} + \Delta i_{hess_k}^T f_{mpc_k}, \tag{34}$$

where

$$H_{mpc_k} = 2\left(\Phi_{mpc_k}^T \Phi_{mpc_k} + K\right),$$

$$f_{mpc_k} = -2\Phi_{mpc_k}^T \left(R_{s_{mpc_k}} - F_{mpc_k} x_{mpc_k} - \varphi_{mpc_k}\right). \tag{35}$$

To efficiently solve the QP problem in real-time applications, the Hildreth's Quadratic Programming Algorithm [33] is employed. The solution of the MPC is given by

$$\Delta u = \begin{bmatrix} \Delta i_{hess_k} & \cdots & \Delta i_{hess_{N_c-1}} \end{bmatrix}^T, \tag{36}$$

where N_c is the control horizon. The control horizon defines the window over which the MPC optimizes the sequence of future control actions.

F. OVERVIEW OF THE SYSTEM OPERATION USING THE MPC

The system operates in conjunction with the MPC. The MPC functions as a high-level controller, determining the system's power operating point by defining the HESS current references: the battery current (i_{bat}^*) and the supercapacitor current (i_{sc}^*). This operation is illustrated in Fig. 3. Initially, the system acquires measurements such as i_{pv_k}, v_{pv_k}, i_{ac_k}, and v_{ac_k}. These measurements are essential for enabling the operation of the low-level controllers that regulate the converters and for calculating the HESS power demand, which is required by the first term in (6).

Other measurements are necessary. The i_{bat_k} and v_{bat_k} are acquired for the determination of the State of Charge (SOC) of the lithium-ion battery using an Extended Kalman Filter (EKF). The MPC uses this SOC in the second term of the cost function (6). Finally, v_{sc_k} is an input to calculate the SOC_{sc} for the third term and the supercapacitor power for the first term of the same equation.

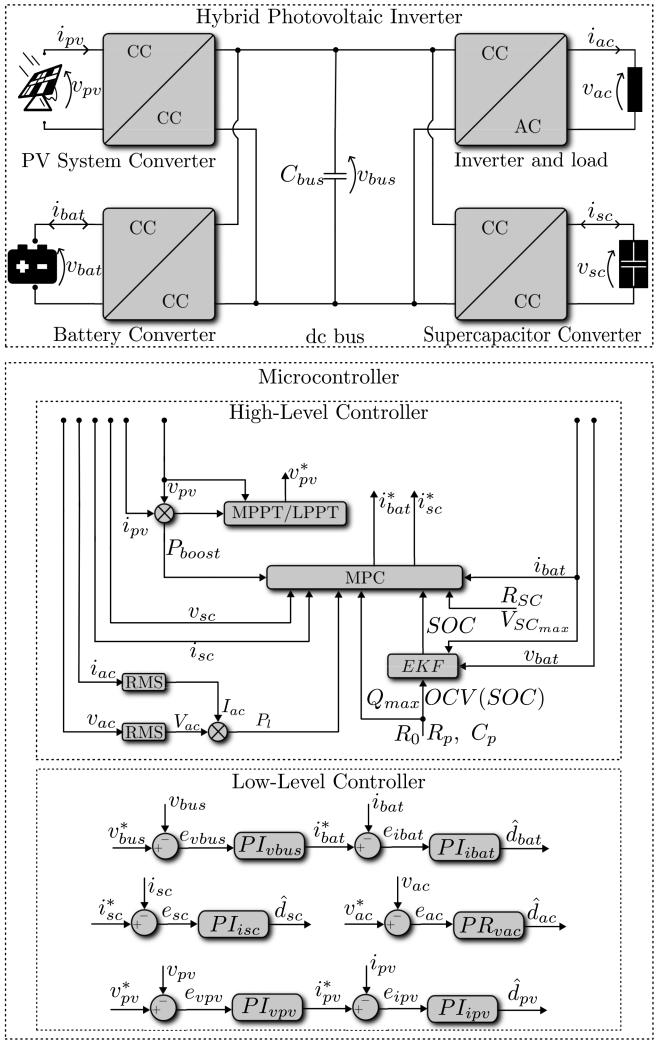

FIGURE 3. Hybrid photovoltaic inverter with supercapacitor and Li-ion battery: a system overview of the operation.

The MPC needs some HESS parameters. For the battery, the MPC requires the parameters of the battery's Equivalent Circuit Model, such as $OCV(SOC)$, R_0, R_P, C_P, and Q_{max}. Methodologies for determining these parameters are demonstrated in [34]. These values are essential for calculating the battery voltage (v_{bat}) given in (4) and, consequently, the battery power in the first term. Finally, the series resistances R_0 (for the Li-ion battery) and R_{SC} (for the supercapacitor) are used to compute the power dissipated within the HESS, as defined in the fourth and fifth terms.

The low-level controllers regulating the system's converters are illustrated in Fig. 3. The first control stage governs the boost converter, which extracts energy from the PV system. To achieve this, the MPPT/LPPT algorithm generates the PV voltage reference (v_{pv}^*). This reference serves as the input for the voltage controller (PI_{vpv}), whose output provides the current reference (i_{pv}^{*}). This reference then feeds the inner current controller (PI_{ipv}), which adjusts the duty cycle to ensure the boost converter tracks the target voltage. Both controllers are of the Proportional-Integral (PI) type. The LPPT mode is activated when the HESS (battery and supercapacitor) is fully charged and the available PV power exceeds the load demand, requiring the generated power to be curtailed to match the consumption. The second control stage manages the inverter. This controller (PR_{vac}) regulates the AC bus voltage (v_{ac}), maintaining it at 127 V_{RMS} and 60 Hz; it is implemented as a Proportional-Resonant (PR) controller.

The third converter is the bidirectional buck-boost converter associated with the battery. This converter is responsible for regulating the bus voltage (v_{bus}). To achieve this, the voltage controller (PI_{vbus}) generates the current reference (i_{bat}^{*}) required to regulate this voltage. This reference feeds the inner current controller (PI_{ibat}), whose output adjusts the duty cycle to maintain the bus voltage at its reference value. Both controllers are of the Proportional-Integral (PI) type. The final controller manages the supercapacitor's bidirectional buck-boost converter. To ensure the supercapacitor current tracks the reference i_{sc}^{*}, a Proportional-Integral (PI_{isc}) controller is implemented, and its output determines the duty cycle required to maintain the current at the reference value.

A crucial consideration must be addressed regarding the system's control hierarchy. Since the battery's bidirectional buck-boost converter is responsible for regulating the DC bus voltage (v_{bus}), the battery current is not under the direct control of the MPC. As illustrated in the control structure in Fig. 3, the v_{bus} voltage controller (PI_{vbus}) generates the battery current reference (i_{bat}^{*}) as its output. While the MPC calculates optimal current references for both the battery and the supercapacitor to balance power generation and load demand as defined in the first term of (6), only the supercapacitor current controller (PI_{isc}) is dedicated to directly tracking its respective reference. Nevertheless, when the PI_{isc} drives the supercapacitor current to the MPC calculated reference (i_{sc}^{*}), the battery current implicitly converges to its own reference (i_{bat}^{*}). This occurs because, by regulating v_{bus}, the battery converter inherently compensates for any remaining power imbalances on the DC bus.

Once all parameters and measurements used by the MPC as inputs are available, as presented in Fig. 3, the sequence of procedures presented in Algorithm 1 is used to define the current references for the battery ($i_{bat_{k+1}}^{*}$) and supercapacitor ($i_{sc_{k+1}}^{*}$).

Initially, in step 1, the state-space model described by (15) and (20), which comprise the matrices A_{mpc}, B_{mpc}, and C_{mpc} is updated. These matrices are used to construct Φ_{mpc} and F_{mpc}, as defined in (23). With these matrices, the system outputs can be predicted in step 2. Also, using these matrices, the constraints are defined, and the constraint matrices M_{mpc} and γ_{mpc} presented in (30) are constructed in step 3.

In Step 4, the quadratic programming (QP) problem is formulated using the Hessian matrix H_{mpc_k} and the gradient vector f_{mpc_k} defined in (35). To solve this optimization under constraints, the Hildreth algorithm explores the primal-dual relationship, where the control action Δi_{hess_k} is analytically linked to the Lagrange multipliers λ by:

Algorithm 1: MPC Power Management Strategy.

Require: Parameters: R_0, R_P, C_P, R_{SC}, $v_{sc_{max}}$, N_P, N_C
Require: Measurements: SOC_k, i_{bat_k}, i_{sc_k}, v_{sc_k}, P_{boost_k}, P_{l_k}

Step 1: Model Update
Build discrete state-space matrices A_{mpc}, B_{mpc}, C_{mpc} based on (15) and (20).
Step 2: Output Predictions
Compute prediction matrices Φ_{mpc_k}, F_{mpc_k} and φ_{mpc_k} defined in (23) and (24).
Step 3: Constraints
Construct constraint matrices M_{mpc_k} and γ_{mpc_k} from (30).
Step 4: Quadratic Programming Setup
Calculate Hessian H_{mpc_k} and gradient f_{mpc_k} presented in (35).
Step 5: QP Hildreth Solver
Solve the optimization problem using the matrices H_{mpc_k}, f_{mpc_k}, M_{mpc_k}, and γ_{mpc_k} defined in (35) and (25).
Obtain the optimal control action from the solution vector $[\Delta i_{hess_k}^T, \ldots, \Delta i_{hess_{N_C-1}}^T]^T$.
Step 6: Obtaining the HESS current references
Using the first solution from Step 5 (Δi_{hess_k}) and (13), the optimal current references for the HESS are obtained.
Step 7: Applying the HESS current references
With the HESS current references, the low-level controllers drive the system toward the optimal operating point.

$$\Delta i_{hess_k} = -H_{mpc_k}^{-1}\left(f_{mpc_k} + M_{mpc_k}^T \lambda\right). \tag{37}$$

The dual problem is then constructed using the following matrices:

$$P_{mpc_k} = M_{mpc_k} H_{mpc_k}^{-1} M_{mpc_k}^T, \tag{38}$$

$$d_{mpc_k} = M_{mpc_k} H_{mpc_k}^{-1} f_{mpc_k} + \gamma_{mpc_k}. \tag{39}$$

The algorithm iteratively updates each component of the multiplier vector w_i^{m+1} through:

$$w_i^{m+1} = -\frac{1}{P_{mpc_k,ii}}\Bigg[d_{mpc_k,i} + \sum_{j=1}^{i-1} P_{mpc_k,ij}\lambda_j^{m+1} + \sum_{j=i+1}^{n} P_{mpc_k,ij}\lambda_j^{m}\Bigg]. \tag{40}$$

To satisfy the Karush-Kuhn-Tucker (KKT) conditions for inequality constraints, the multipliers are projected onto the non-negative orthant:

$$\lambda_i^{m+1} = \max\left(0, w_i^{m+1}\right). \tag{41}$$

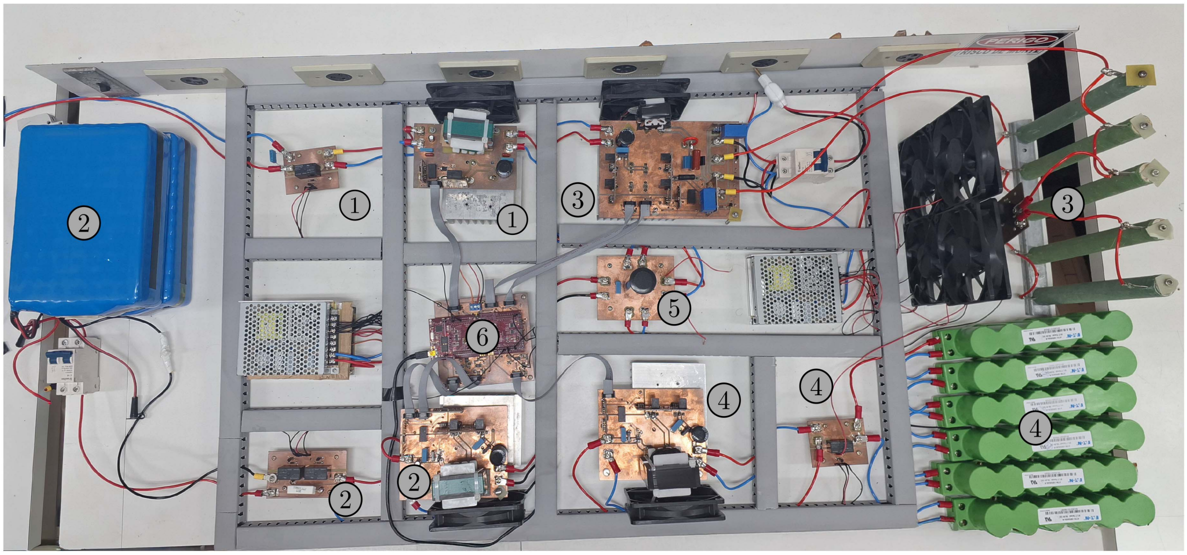

FIGURE 4. Experimental setup of the hybrid photovoltaic inverter: (1) PV system emulator and boost converter; (2) battery's bidirectional buck-boost converter and Li-ion pack; (3) inverter and AC load; (4) supercapacitor's bidirectional buck-boost converter and SC bank; (5) DC bus; and (6) TMS320F28379D microcontroller.

The optimal vector λ^* is reached when the variation between iterations falls below a tolerance ϵ:

$$\lambda^* = \lambda^{m+1} \quad \text{s.t.} \quad \max_i \left|\lambda_i^{m+1} - \lambda_i^m\right| \le \epsilon. \tag{42}$$

Finally, the optimal control increment $\Delta i^*_{hess_k}$ is recovered as:

$$\Delta i^*_{hess_k} = -H^{-1}_{mpc_k} f_{mpc_k} - H^{-1}_{mpc_k} M^T_{mpc_k} \lambda^*. \tag{43}$$

Once the variations in battery and supercapacitor currents are determined using the Hildreth QP solver, the optimum solution is evaluated in Step 6. This stage describes the variation of the HESS current using (7) and updates the current references as:

$$i^*_{bat_{k+1}} = \Delta i_{bat_k} + i_{bat_k}, \tag{44}$$

$$i^*_{sc_{k+1}} = \Delta i_{sc_k} + i_{sc_k}. \tag{45}$$

In Step 7, the $PI_{i_{sc}}$ controller tracks the supercapacitor current reference ($i^*_{sc,k+1}$) calculated by the MPC. Consequently, the Li-ion battery is guided to its current reference by the $PI_{v_{bus}}$ controller.

V. RESULTS

This section presents the experimental results of the proposed MPC-based power management strategy. The algorithm was implemented using the TMS320F28379D dual-core microcontroller; the first CPU (CPU1) is used for the low-level converter control, while the second CPU (CPU2) is dedicated to the high-level MPC power management. The experimental setup, illustrated in Fig. 4, is organized into six primary areas: (1) the boost converter connected to an ITech IT6018C-800-60 power supply used to emulate the PV system; (2) the battery's bidirectional buck-boost converter and the Li-ion battery pack; (3) the inverter connected to the load; (4) the supercapacitor's bidirectional buck-boost converter and the bank of six series-connected supercapacitors; (5) the DC bus; and (6) the TMS320F28379D microcontroller, which coordinates the entire system. The system specifications described in Section II are presented in Table 1.

TABLE 1. System Parameters and Specifications

Parameter	Specification
PV Array	
Parameter	**Specification**
Model	4x CS6U-330P (Series)
V_{mp}	148.8 V
I_{mp}	8.88 A
Supercapacitor Bank	
Parameter	**Specification**
Model	6x XTM-18R0626-R
C_{sc}	10.283 F
$v_{sc_{max}}$	108 V
$i_{sc_{max}}$	20 A
ESR (R_{sc})	0.132 Ω
E_{max}	16.66 Wh
Battery Pack	
Parameter	**Specification**
Model	ICR18650-22F (26S9P)
$v_{bat_{nom}}$	96 V
$i_{bat_{max}}$	20 A
Inverter & DC Bus	
Parameter	**Specification**
v_{ac}	127 V
f_{ac}	60 Hz
V_{bus}	250 V
C_{bus}	1200μF

The MPC parameters, detailed in Section IV, were configured with a prediction horizon of $N_p = 10$ and a control

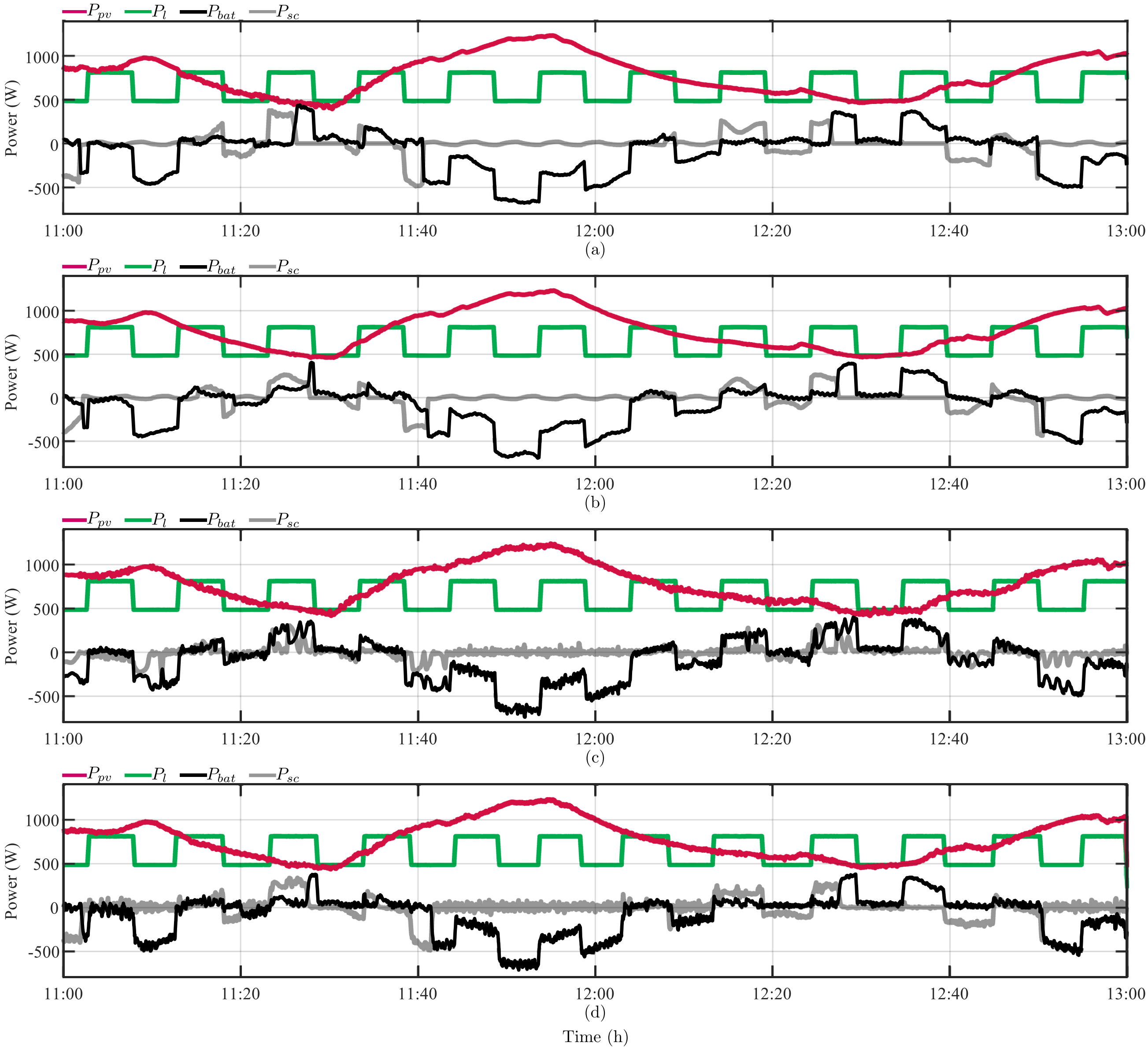

FIGURE 5. Experimental results for the different power management strategies: (a) rule-based; (b) frequency-based; (c) benchmark MPC. (d) Proposed MPC.

horizon of $N_c = 2$. The MPC operates with a sampling interval of $T_{s_{mpc}} = 1$ s (1 Hz), resulting in a total prediction window of 10 seconds. The weighting factors for the cost function (6) were assigned as follows: $\alpha_1 = 1, \alpha_2 = 1, \alpha_3 = 1, \alpha_4 = 200$, and $\alpha_5 = 1$. The weight α_4 is intentionally prioritized because it governs the power dissipation within the Li-ion battery. By heavily penalizing this term, the MPC prioritizes minimizing battery losses, thereby reducing current demand and mitigating operational stress. Additionally, the weighting matrix K for the control action increments is set to the identity matrix, ensuring equal penalties for the variation of the control actions across both storage elements.

The proposed MPC power management is compared to three other strategies. The first one uses a rule-based approach proposed in [35], which prioritizes the supercapacitor over the battery. The second strategy used for comparison is a frequency-based approach that employs an adaptive cutoff frequency to filter the power demand [15]. The third strategy also uses MPC [23], where the main idea is to set the supercapacitor's SOC reference to 50% to keep it available for transient responses.

The powers of all four converters of the hybrid photovoltaic inverter can be seen in Fig. 5. Fig. 5(a) presents the results of the rule-based power management, Fig. 5(b) presents the results of the frequency-based power management, Fig. 5(c) represents the compared MPC and Fig. 5(d) presents the proposed power management using the MPC.

It is possible to observe the boost converter power (P_{pv}) changing in response to the irradiance profile. This profile remains the same for the three results. These results also show

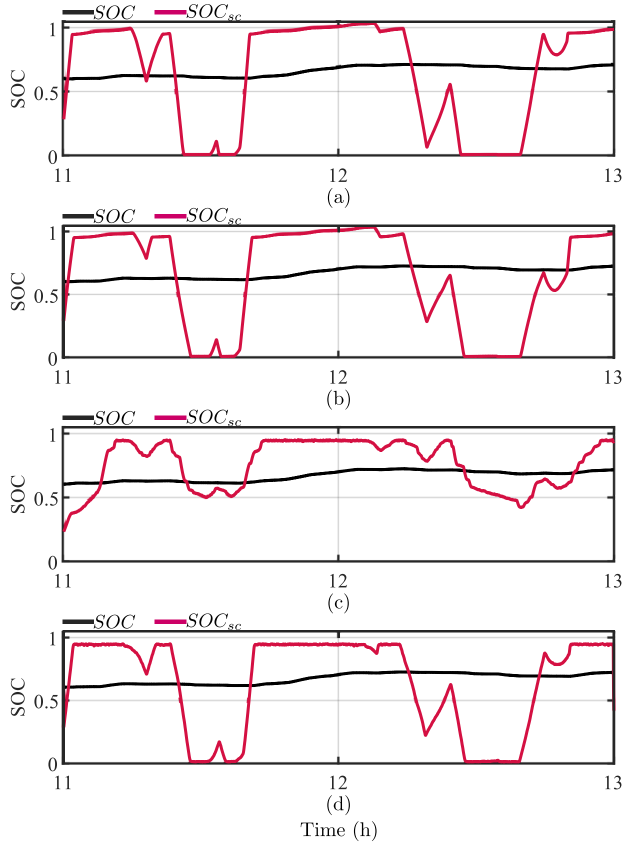

FIGURE 6. State of Charge of the Li-ion battery (*SOC*) and the supercapacitor (*SOC_{sc}*): (a) rule-based management; (b) frequency-based management; (c) benchmark MPC. (d) proposed MPC.

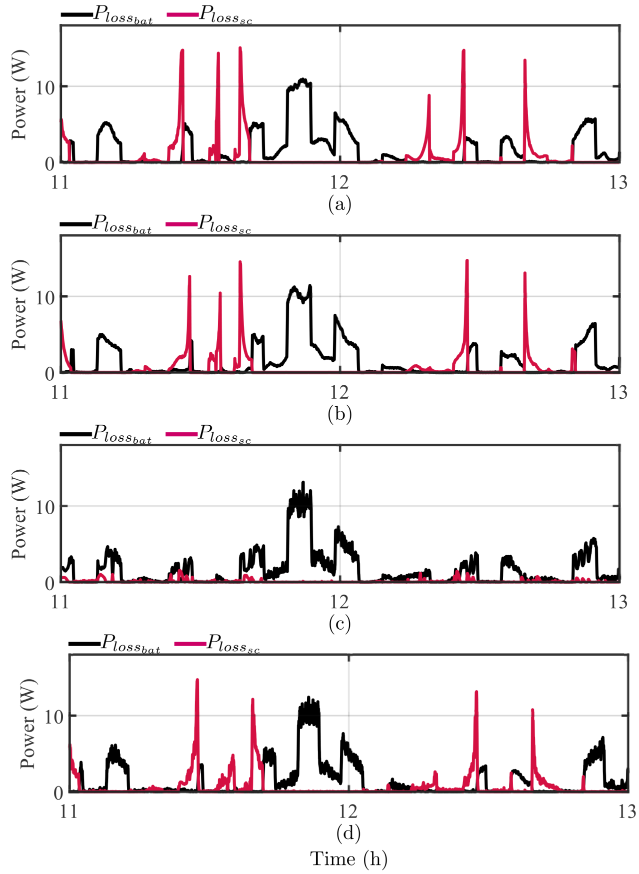

FIGURE 7. Power dissipated in the Li-ion battery and the supercapacitor: (a) rule-based management; (b) frequency-based management; (c) benchmark MPC. (d) proposed MPC.

the load power (P_l), which was intentionally varied to test the robustness of the power management strategies. The load varies between 474 W and 823 W, changing every 300 s. Finally, it is possible to see the battery (P_{bat}) and supercapacitor (P_{sc}) powers varying between positive and negative values. Negative power indicates that the HESS is charging, while positive power means it is discharging.

Fig. 6 illustrates the SOC of the HESS for the four experimental tests. It is evident that SOC_{sc} fluctuates more significantly than the battery SOC due to the supercapacitor's high power density and low energy density. In the rule-based management strategy, the battery SOC varied from 60.31% to 71.56%. Conversely, in the frequency-based management, the variation ranged from 60.37% to 72.71%. In the benchmark MPC, the SOC changed from 60.39% to 72.55%. Finally, in the proposed power management strategy, the SOC varied from 60.37% to 72.34%.

Using the Equivalent Full Cycles (EFC) metric presented in [36], it is possible to analyze which method results in the lowest battery cycling. The EFC is represented by:

$$EFC = \frac{1}{2Q_{nom}} \left(\int_{t_0}^{t_f} |i_{bat_{ch}}(t)| \, dt + \int_{t_0}^{t_f} |i_{bat_{dis}}(t)| \, dt \right), \tag{46}$$

where Q_{nom} is the nominal capacity of the battery, while $i_{\text{bat,ch}}$ and $i_{\text{bat,dis}}$ represent the battery's charging and discharging currents, respectively. The Ah throughput of charging and discharging is summed to obtain the EFC.

The rule-based management yields a partial cycle usage of 17.15%, the frequency-based management yields 16.59%, and the benchmark MPC strategy yields 18.58%. In comparison, the proposed MPC achieved only 14.38%. The proposed MPC significantly reduces battery cycling, thereby mitigating degradation.

Fig. 7 illustrates the power losses within the HESS (Li-ion battery and supercapacitor). Comparing the supercapacitor's energy dissipation across the four strategies, the rule-based management dissipated 0.652 Wh, the frequency-based method dissipated 0.518 Wh, the benchmark MPC dissipated 0.085 Wh, and the proposed MPC dissipated 0.597 Wh. The proposed MPC does not exhibit the lowest supercapacitor power loss. This occurs because the MPC is formulated to prioritize the reduction of battery stress over supercapacitor losses by setting the weighting factor $\alpha_4 = 200$ in the cost function, as detailed in Section IV.

Regarding the battery's energy dissipation, the proposed MPC power management strategy demonstrates superior performance. The battery energy loss using the rule-based

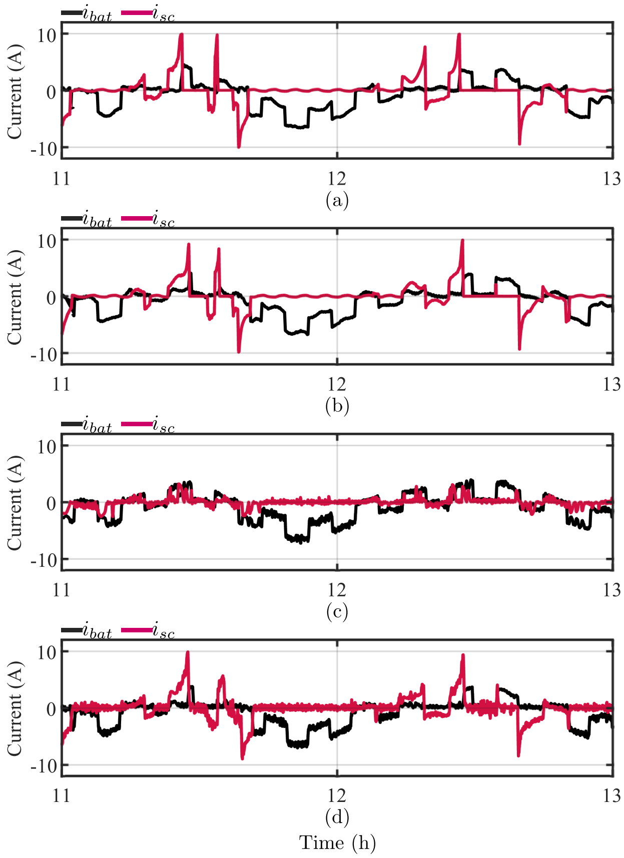

FIGURE 8. Currents of the Li-ion battery and the supercapacitor: (a) rule-based management; (b) frequency-based management; (c) benchmark MPC. (d) proposed MPC.

strategy is 1.583 Wh, identical to the benchmark MPC (1.583 Wh), whereas the frequency-based strategy results in 1.473 Wh. In contrast, the proposed MPC strategy achieves an energy loss of only 1.387 Wh. This represents a reduction in battery energy losses of 12.38% when benchmark to both the rule-based and benchmark MPC strategies, and a 5.84% improvement over the frequency-based approach.

Finally, regarding the total HESS energy losses (the sum of battery and supercapacitor dissipation), the proposed MPC does not exhibit the most efficient global indicators. The rule-based management results in a total loss of 2.235 Wh, while the frequency-based approach dissipates 1.99 Wh. The benchmark MPC achieves the lowest total loss at 1.668 Wh, whereas the proposed strategy results in 1.984 Wh. Compared to the rule-based strategy, the proposed MPC achieves an 11.23% reduction in total energy loss. However, compared to the benchmark MPC, the proposed method results in a 18.94% increase in total dissipation. This performance degradation in global efficiency is a deliberate trade-off. As previously discussed, the proposed strategy prioritizes battery health and lifespan by mitigating operational stress and shifting power-demand transients to the more robust supercapacitor.

Fig. 8 displays the current profiles for the Li-ion battery (i_{bat}) and the supercapacitor (i_{sc}) across the four experimental tests. Notably, the peak supercapacitor current reaches 10 A in the rule-based, frequency-based, and proposed MPC scenarios. This does not compromise system performance, given the supercapacitor's high power density. To evaluate the operational stress on the battery, the Root Mean Square (RMS) current of i_{bat} is analyzed, as it directly reflects the thermal and structural degradation of the cells [37]. The proposed MPC strategy achieves the lowest RMS current at 2.356 A. Compared to both the rule-based and benchmark MPC strategies (2.517 A), this represents a 6.40% reduction; compared to the frequency-based method (2.427 A), the reduction is 2.93%. Consequently, the proposed MPC provides a smoother current profile, significantly mitigating the impact on the battery's lifespan.

To determine which strategy minimizes battery degradation, the State of Health (SOH) loss (ΔSOH) is calculated using (47) [38]. This factor accounts for the non-linear nature of degradation across the SOC range; specifically, operating near 50% SOC results in lower degradation than operating near the charge or discharge extremes. The Li-ion battery's SOH degradation is quantified in the four experimental tests using

$$\Delta SOH(\%) = \frac{100}{2 \cdot Q_{nom} \cdot N_{life}} \sum_{t=1}^{k} |I(t)| \cdot \Delta t \cdot \gamma_{SOC}(t)$$

$$\gamma_{SOC}(t) = 1 + 0.5 \cdot (SOC(t) - 0.5)^2. \tag{47}$$

The proposed MPC exhibits the lowest Li-ion battery degradation (ΔSOH). Specifically, the rule-based strategy resulted in a ΔSOH of 0.0003478%, while the frequency-based approach yielded 0.0003370%. The benchmark MPC showed the highest degradation at 0.0003773%. In contrast, the proposed MPC achieved the lowest value of 0.0002920%. These results demonstrate that the proposed strategy successfully mitigates battery degradation when employed in the hybrid photovoltaic inverter.

Fig. 9 illustrates the superior performance of the proposed MPC compared to the other three strategies. In this analysis, lower values indicate better performance. It is evident that the proposed MPC outperforms the others in terms of Equivalent Full Cycles (EFC), RMS current, and battery degradation (ΔSOH). However, it does not yield the lowest power losses in the HESS. This outcome is expected, as the cost function weights are tuned to minimize battery usage by shifting the load to the supercapacitor. Consequently, the power losses in the supercapacitor are higher than those observed in the benchmark MPC.

While the experimental results spanned two hours, a seven-day simulation was conducted to facilitate a long-term comparison using real irradiance profiles from 08:00 to 18:00. The SOC of the storage elements was reset at the beginning of each day throughout the simulation. Fig. 10 presents these results: Fig. 10(a) displays the Li-ion battery cycle usage (EFC), Fig. 10(b) illustrates the total energy

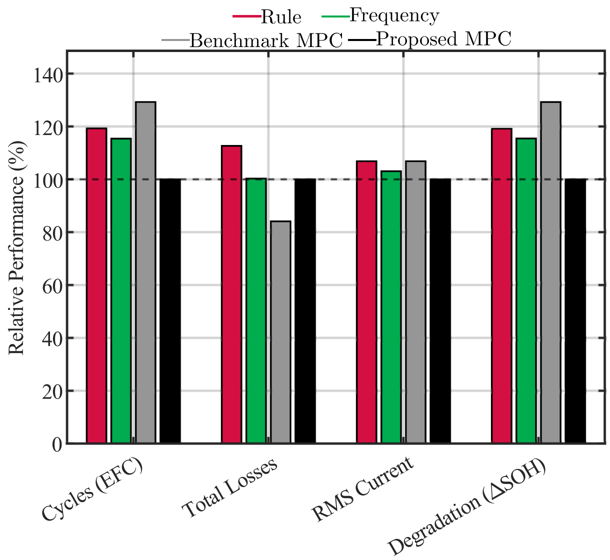

FIGURE 9. Comparison of performance metrics across the strategies: Equivalent Full Cycles (EFC), Power Losses, RMS Current, and Battery Degradation (ΔSOH).

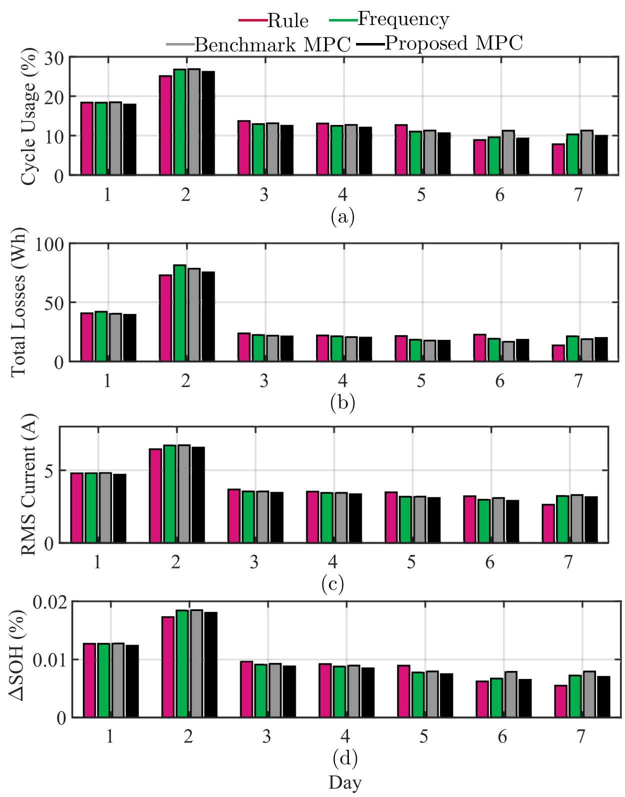

FIGURE 10. Simulation results over a seven-day period using real irradiance profiles: (a) Li-ion battery cycle usage (EFC); (b) Energy loss in the HESS; (c) RMS current comparison; (d) Degradation (ΔSOH).

losses in the HESS, Fig. 10(c) depicts the daily RMS current, and Fig. 10(d) illustrates the resulting battery degradation (ΔSOH). Regarding the battery cycling, the proposed MPC demonstrated reductions of 1.13% compared to the rule-based strategy, 2.92% compared to the frequency-based

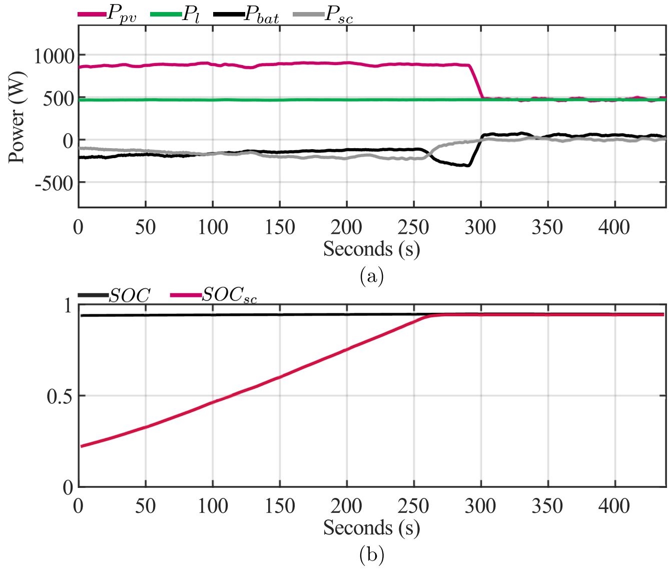

FIGURE 11. Experimental results of the system under the Limited Power Point Tracking (LPPT) mode: (a) Comparison of system power profiles; (b) Battery and supercapacitor state of charge.

strategy, and a significant 6.17% reduction compared to the benchmark MPC. In terms of energy losses, the proposed strategy yielded reductions of 2.39%, 6.23%, and 1.14% relative to the rule-based, frequency-based, and benchmark methods, respectively. Concerning the RMS current, the proposed MPC achieved a reduction of 2.15% compared to the rule-based strategy, 2.51% compared to the frequency-based strategy, and 3.26% compared to the benchmark MPC. Finally, regarding the battery degradation (ΔSOH), the proposed MPC achieved reductions of 2.30%, 2.75%, and 4.44% compared to the rule-based, frequency-based, and benchmark methods, respectively.

The results presented in Fig. 11 illustrate the activation of the LPPT mode. When power generation exceeds the load demand, and the HESS is fully charged, the excess energy cannot be stored. Consequently, the only viable solution is to activate the Limited Power Point Tracking (LPPT) algorithm. However, this activation occurs externally to the MPC, as the MPC's scope is limited to managing the battery (i_{bat}) and supercapacitor (i_{sc}) currents. The power reference for the LPPT is set to the load power (P_l), a variable that is already available and required by the MPC. Initially, the system charges the supercapacitor and the battery. Once fully charged, the PV power generation (P_{pv}) is curtailed to match the load power (P_l), maintaining the HESS current near zero. Since LPPT is an iterative algorithm, the match between P_{pv} and P_l is not perfect; consequently, the battery compensates for the resulting power difference.

The final results illustrate the transient response of the four management strategies during a load step change, specifically analyzing the HESS currents (i_{bat} and i_{sc}), the bus voltage (v_{bus}), and the load current (i_{ac}). These results are crucial for interpreting the interaction between control layers with

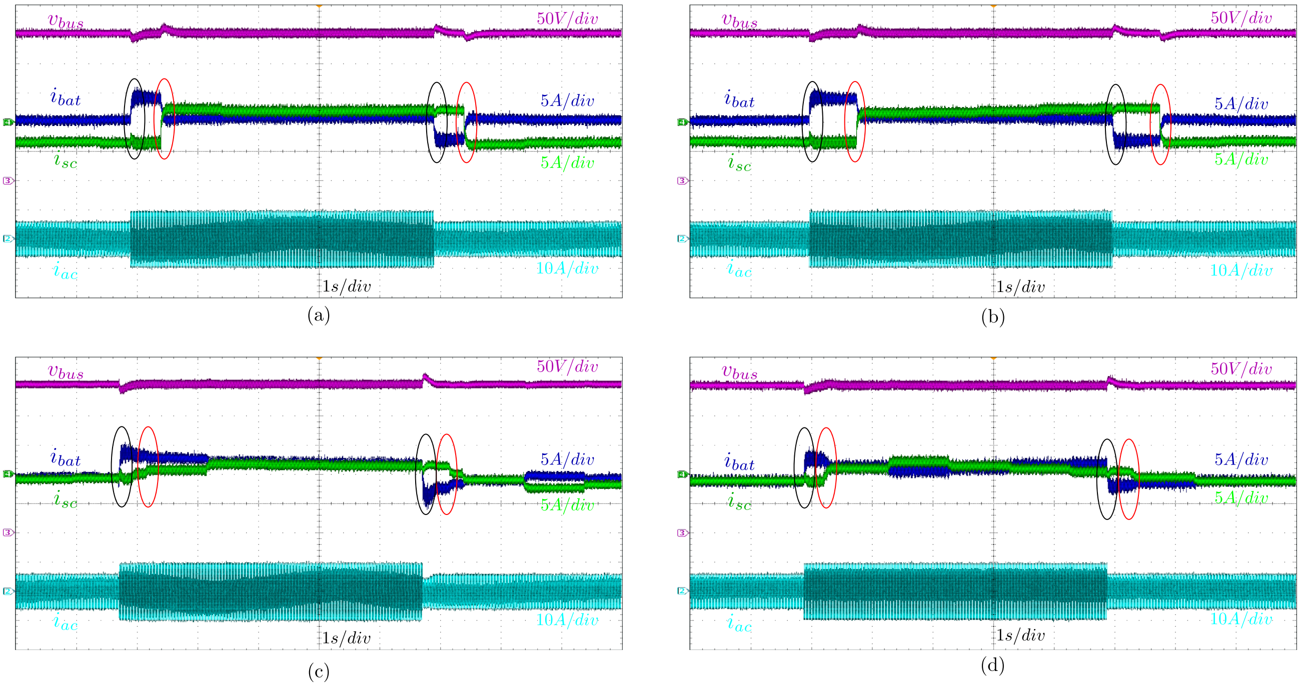

FIGURE 12. Experimental results showing the transient response of HESS currents (i_{bat}, i_{sc}), bus voltage (v_{bus}), and load current (i_{ac}) during a load step change. Black circles indicate the immediate low-level voltage regulation response, while red circles mark the high-level PMS update delay. (a) rule-based management; (b) frequency-based management; (c) benchmark MPC. (d) proposed MPC.

different time scales; for instance, the low-level controllers shown in Fig. 3 operate at 100k Hz, whereas the proposed power management strategies operate at 1 Hz. As highlighted by the black circles in Fig. 12(a), 12(b), 12(c), and 12(d), when the load changes, the low-level bus voltage controller reacts immediately. Consequently, the battery inherently compensates for the power difference by adjusting its current. This phenomenon occurs in all four tests and is an intrinsic behavior of the low-level voltage regulation loop.

Following the load change (black circles), the high-level power management system updates its control action after a delay of some milliseconds (indicated by red circles). In the rule-based and frequency-based strategies, this decision results in a significant step change in battery current. In contrast, both MPC strategy behaves differently. When the load changes and the algorithm updates its decision, the current demand is effectively distributed between the battery and the supercapacitor. However, the proposed strategy utilizes the battery less intensely, as evidenced by its lower current amplitude. This distribution significantly reduces the magnitude of the step change in the battery current, thereby mitigating battery stress.

VI. CONCLUSION

This paper presented an enhanced power management strategy based on Model Predictive Control (MPC) for an off-grid hybrid photovoltaic inverter integrated with a Hybrid Energy Storage System (HESS). The work introduced two primary contributions: a novel controller formulation that explicitly penalizes battery internal power dissipation within the cost function and an extensive experimental validation framework. The proposed strategy was designed to prioritize mitigating physical stress and operational degradation in Lithium-ion batteries by optimizing power-sharing with supercapacitors.

The performance of the proposed MPC was rigorously evaluated through a comparative analysis with three established strategies: rule-based, frequency-based, and a benchmark MPC. Results were analyzed across four key metrics, including RMS current, total power losses, Equivalent Full Cycles (EFC), and State of Health variation (ΔSOH). Experimental results demonstrated that the proposed MPC significantly reduces battery stress, outperforming the benchmark strategies in terms of cycling and current distribution. Furthermore, the proposed method yielded lower RMS current values, confirming its ability to provide a well-behaved and less aggressive operating regime for the battery cells.

Long-term simulations utilizing real irradiance profiles corroborated the experimental findings, showing a substantial reduction in battery degradation compared to the benchmark approaches. While the strategy focuses on mitigating battery degradation, it also maintains a balanced performance regarding total power losses across the HESS, demonstrating robustness for high-performance off-grid applications. In conclusion, the combination of an optimized cost function and rigorous experimental evidence confirms that the proposed MPC is an effective tool for mitigating battery degradation. This work demonstrates that penalizing internal dissipation is a viable approach to enhancing the reliability of hybrid energy storage systems without compromising overall system efficiency.

REFERENCES

[1] M. Habibzadeh, M. Hassanalieragh, A. Ishikawa, T. Soyata, and G. Sharma, "Hybrid solar-wind energy harvesting for embedded applications: Supercapacitor-based system architectures and design tradeoffs," *IEEE Circuits Syst. Mag.*, vol. 17, no. 4, pp. 29–63, 4th Quart. 2017.

[2] E. L. Carvalho, A. Chub, N. Hassanpour, A. Blinov, A. K. Rathore, and D. Vinnikov, "P^3R: Partial power postregulated grid-forming converter for prosumer DC buildings," *IEEE Trans. Ind. Electron.*, vol. 72, no. 2, pp. 1628–1637, Feb. 2025.

[3] E. Zarate-Perez, E. Rosales-Asensio, A. González-Martıńez, M. de Simón-Martıń, and A. Colmenar-Santos, "Battery energy storage performance in microgrids: A scientific mapping perspective," *Energy Rep.*, vol. 8, pp. 259–268, 2022.

[4] X. Zhang et al., "Decentralized control of multiple supercapacitors for hybrid energy storage converter in off-grid mode under power fluctuations and short-time high power," *IEEE Trans. Ind. Appl.*, vol. 60, no. 5, pp. 7225–7239, Sep./Oct. 2024.

[5] E. L. Carvalho, A. Chub, A. Blinov, S. N. Banavath, and D. Vinnikov, "Magnetically integrated multiport converter for energy management in DC-powered buildings," *Eletrônica de Potência*, vol. 29, Nov. 2024, Art. no. e452024.

[6] S. Sahoo and P. Timmann, "Energy storage technologies for modern power systems: A detailed analysis of functionalities, potentials, and impacts," *IEEE Access*, vol. 11, pp. 49689–49729, 2023.

[7] B. P. Roberts and C. Sandberg, "The role of energy storage in development of smart grids," *Proc. IEEE*, vol. 99, no. 6, pp. 1139–1144, Jun. 2011.

[8] D. Li et al., "The effect of electrode thickness on the high-current discharge and long-term cycle performance of a lithium-ion battery," *Batteries*, vol. 8, no. 8, 2022, Art. no. 101.

[9] D. Yousefi and A. Soleymani, "Circular economy and sustainability in lithium-ion battery development in China and the USA," *World Electric Veh. J.*, vol. 16, no. 10, 2025, Art. no. 578.

[10] L. H. Meneghetti et al., "Multifunctional PV converter for uninterrupted power supply," in *Proc. IEEE PES Innov. Smart Grid Technol. Conf. - Latin Amer.*, 2019, pp. 1–6.

[11] E. Gonschorowski et al., "MPC based power management for off-grid photovoltaic hybrid inverters using li-ion batteries and supercapacitors," in *Proc. IEEE 7th Int. Conf. DC Microgrids*, 2025, pp. 1–6.

[12] A. S. Mohammed, S. M. Atnaw, A. O. Salau, and J. N. Eneh, "Review of optimal sizing and power management strategies for fuel cell/battery/super capacitor hybrid electric vehicles," *Energy Rep.*, vol. 9, pp. 2213–2228, 2023.

[13] E. Gonschorowski et al., "Analysis of the use of supercapacitors and batteries as energy storage elements for off-grid hybrid photovoltaic inverters," in *Proc. IEEE 8th Southern Power Electron. Conf. 17th Braz. Power Electron. Conf.*, 2023, pp. 1–7.

[14] E. L. Carvalho, L. V. Bellinaso, R. Cardoso, and L. Michels, "Distributed price-based power management for multibuses DC nanogrids EEMS," *IEEE Trans. Emerg. Sel. Topics Power Electron.*, vol. 10, no. 5, pp. 5509–5521, Oct. 2022.

[15] E. Gonschorowski et al., "Adaptive frequency-based power management for off-grid hybrid photovoltaic converters," *Eletrônica de Potência*, vol. 29, pp. e202440–e202440, 2024.

[16] S. A. Zaid, H. Albalawi, H. M. El-Hageen, A. Wadood, and A. Bakeer, "Stabilization of DC microgrids using frequency-decomposed fractional-order control and hybrid energy storage," *Fractal Fractional*, vol. 9, no. 10, 2025, Art. no. 670.

[17] F. Härtel and T. Bocklisch, "Minimizing energy cost in PV battery storage systems using reinforcement learning," *IEEE Access*, vol. 11, pp. 39855–39865, 2023.

[18] G. Moorthy, S. Vijayalakshmi, A. Manjuladevi, and M. Anusuya, "Advanced energy management and power quality enhancement in hybrid fuel cell-battery-super capacitor microgrids using snow ablation optimizer-robust variational physics informed," *J. Energy Storage*, vol. 116, 2025, Art. no. 115859.

[19] M. R. Larijani, S. H. Kia, M. Zolghadri, A. El Hajjaji, and A. Taghavipour, "Linear parameter-varying model predictive control for intelligent energy management in battery/supercapacitor electric vehicles," *IEEE Access*, vol. 12, pp. 51026–51040, 2024.

[20] A. Mallick, A. Mondal, A. R. Hota, D. Kastha, and P. Bajpai, "Hybrid model predictive control framework for efficient operation of a five-port converter interfaced DC microgrid," *IEEE Trans. Ind. Electron.*, vol. 72, no. 7, pp. 6969–6979, Jul. 2025.

[21] S. Sen and M. Kumar, "Distributed-MPC type optimal EMS for renewables and EVs based grid-connected building integrated microgrid," *IEEE Trans. Ind. Appl.*, vol. 60, no. 2, pp. 2390–2408, Mar./Apr. 2024.

[22] S. A. G. K. Abadi, S. I. Habibi, T. Khalili, and A. Bidram, "A model predictive control strategy for performance improvement of hybrid energy storage systems in DC microgrids," *IEEE Access*, vol. 10, pp. 25400–25421, 2022.

[23] I. Pervez, C. Antoniadis, and H. Ghazzai, "Computationally efficient model predictive control for enhanced primary-level management of standalone microgrids with hybrid storage systems," *IEEE Trans. Sustain. Energy*, vol. 16, no. 4, pp. 2586–2599, Oct. 2025.

[24] X. Zhang, B. Wang, D. Gamage, and A. Ukil, "Model predictive control based dynamic power loss prediction for hybrid energy storage system in DC microgrids," *IEEE Trans. Ind. Electron.*, vol. 69, no. 8, pp. 8080–8090, Aug. 2022.

[25] X. Liu, Y. Suo, Z. Zhang, X. Song, and J. Zhou, "A new model predictive current control strategy for hybrid energy storage system considering the SOC of the supercapacitor," *IEEE Trans. Emerg. Sel. Topics Power Electron.*, vol. 11, no. 1, pp. 325–338, Feb. 2023.

[26] J. Snoussi, S. B. Elghali, M. Benbouzid, and M. F. Mimouni, "Optimal sizing of energy storage systems using frequency-separation-based energy management for fuel cell hybrid electric vehicles," *IEEE Trans. Veh. Technol.*, vol. 67, pp. 9337–9346, Oct. 2018.

[27] C. C. dos Santos, C. F. Moraes, J. P. da Costa, C. M. Stein, E. G. Carati, and R. Cardoso, "Photovoltaic boost converter control operating in the mppt and lppt modes," in *Proc. IEEE 15th Braz. Power Electron. Conf. 5th IEEE Southern Power Electron. Conf.*, 2019, pp. 1–6.

[28] E. Gonschorowski et al., "Analysis of the use of supercapacitors and batteries as energy storage elements for off-grid hybrid photovoltaic inverters," in *Proc. IEEE 8th Southern Power Electron. Conf. 17th Braz. Power Electron. Conf.*, 2023, pp. 1–7.

[29] H. Ramadan, M. Becherif, and F. Claude, "Extended Kalman filter for accurate state of charge estimation of lithium-based batteries: A comparative analysis," *Int. J. Hydrogen Energy*, vol. 42, no. 48, pp. 29033–29046, 2017.

[30] R. Zhang et al., "A study on the open circuit voltage and state of charge characterization of high capacity lithium-ion battery under different temperature," *Energies*, vol. 11, no. 9, 2018, Art. no. 2408.

[31] K. S. Holkar and L. M. Waghmare, "An overview of model predictive control," *Int. J. Control Automat.*, vol. 3, no. 4, pp. 47–63, 2010.

[32] M. Yang, X. Sun, R. Liu, L. Wang, F. Zhao, and X. Mei, "Predict the lifetime of lithium-ion batteries using early cycles: A review," *Appl. Energy*, vol. 376, 2024, Art. no. 124171.

[33] L. Wang, *Model Predictive Control System Design and Implementation Using MATLAB*, vol. 3. Berlin, Germany: Springer, 2009.

[34] P. Poopanya, K. Sivalertporn, and T. Phophongviwat, "A comparative study on the parameter identification of an equivalent circuit model for an Li-ion battery based on different discharge tests," *World Electr Veh. J.*, vol. 13, no. 3, pp. 1–17, 2002.

[35] H. Guentri, T. Allaoui, M. Mekki, and M. Denai, "Power management and control of a photovoltaic system with hybrid battery-supercapacitor energy storage based on heuristics methods," *J. Energy Storage*, vol. 39, 2021, Art. no. 102578.

[36] S. N. Motapon, E. Lachance, L.-A. Dessaint, and K. Al-Haddad, "A generic cycle life model for lithium-ion batteries based on fatigue theory and equivalent cycle counting," *IEEE Open J. Ind. Electron. Soc.*, vol. 1, pp. 207–217, 2020.

[37] J. Qu, Z. Jiang, and J. Zhang, "Investigation on lithium-ion battery degradation induced by combined effect of current rate and operating temperature during fast charging," *J. Energy Storage*, vol. 52, 2022, Art. no. 104811.

[38] W. Xu et al., "Data-driven semi-empirical model approximation method for capacity degradation of retired lithium-ion battery considering SOC range," *Appl. Sci.*, vol. 13, no. 21, 2023, Art. no. 11943.

EZEQUIEL GONSCHOROWSKI received the B.Sc. and M.Sc. degrees in electrical engineering from the Federal University of Technology – Paraná (UTFPR), Pato Branco, Brazil, in 2022 and 2025, respectively. His research focuses on hybrid inverter management to maximize battery lifespan and the application of model predictive control (MPC) in energy storage systems.

RAFAEL CARDOSO received the B.S. degree in electrical engineering from the Federal University of Santa Maria (UFSM), Santa Maria, Brazil, in 2001, the M.Sc. degree from the Technological Institute of Aeronautics (ITA), São Paulo, Brazil, in 2003, and the Ph.D. degree in electrical engineering from UFSM, in 2008. Since 2006, he has been with the Federal University of Technology – Paraná (UTFPR), Pato Branco, Brazil, where he is currently a Full Professor. His research interests include control systems, power electronics, energy storage systems, and smart grids.

EDIVAN LAERCIO CARVALHO (Senior Member, IEEE) received the B.Sc. and M.Sc. degrees in electrical engineering from the Federal University of Technology—Paraná, Pato Branco, Brazil, in 2015 and 2018, respectively, and the Ph.D. degree in electrical engineering from the Federal University of Santa Maria, Santa Maria, Brazil, in 2021. Since 2025, he has been an Assistant Professor with the Faculty of Science and Technology, NOVA University of Lisbon, Lisbon, Portugal. He is also a Researcher with Power Electronics Group, Tallinn University of Technology, Tallinn, Estonia. His research interests include high-frequency power converter topologies, net-zero energy buildings, and advanced power management systems.

CARLOS MARCELO DE OLIVEIRA STEIN received the B.S., M.Sc., and Ph.D. degrees in electrical engineering from the Federal University of Santa Maria, Santa Maria, Brazil, in 1996, 1997, and 2003, respectively. Since 2003, he has been with the Federal University of Technology – Paraná (UTFPR), Pato Branco, Brazil, where he is currently a Professor. His research interests include high-frequency power converter topologies, distributed generation, and soft-switching techniques.

EMERSON GIOVANI CARATI received the B.S., M.Sc., and Ph.D. degrees in electrical engineering from the Federal University of Santa Maria (UFSM), Santa Maria, Brazil, in 1996, 1999, and 2003, respectively. Since 2003, he has been with the Federal University of Technology – Paraná (UTFPR), Pato Branco, Brazil, where he is currently a Full Professor. His research interests include control of electrical machine drives, distributed power generation, and static converters.

GUSTAVO WEBER DENARDIN received the B.S., M.Sc., and Ph.D. degrees in electrical engineering from the Federal University of Santa Maria, Santa Maria, Brazil, in 2002, 2004, and 2012, respectively. Since 2005, he has been with the Federal University of Technology – Paraná (UTFPR), Pato Branco, Brazil, where he is currently a Full Professor. His research interests include embedded systems, real-time operating systems, wireless sensor/actuator networks, and smart grids.

JEAN PATRIC DA COSTA received the B.S. degree in electrical engineering, and the M.Sc. and Ph.D. degrees from the Federal University of Santa Maria, Santa Maria, Brazil, in 2004, 2006, and 2010, respectively. He is currently a Professor with the Department of Electrical Engineering, Federal University of Technology – Paraná (UTFPR), Pato Branco, Brazil. His research interests include the control of static converters, smart grids, ancillary services, and distributed generation systems.

Coordenação de Aperfeiçoamento de Pessoal de Nível Superior (CAPES) - ROR identifier: 00x0ma614